JOURNAL OF MATERIALS SCIENCE 14 (1979) 2929–2936

δ-FeO(OH) and its solid solutions

Part 1 *Preparation and crystal chemistry*

OLAF MULLER, ROBERT WILSON*, WILLIAM KRAKOW†
Xerox Corporation, Xerox Square, W114, Rochester, New York 14644, USA

δ-FeO(OH)-type solid solutions have been synthesized with compositions $Fe_{1-x}M_xO_{1-x}(OH)_{1+x}$ ranging up to $x = 0.10$ for M = Ca, $x = 0.35$ for M = Mg or Cd and $x = 0.40$ for M = Zn. The phases are characterized by X-ray diffraction and transmission electron microscope studies. A structural model giving satisfactory intensity agreement is postulated for $Fe_{1-x}Zn_xO_{1-x}(OH)_{1+x}$. In this model, Zn^{2+} ions are situated in the 0 0 0 octahedral sites of space group $D^3_{3d} - P\bar{3}m1$ while the Fe^{3+} ions are almost equally distributed among both octahedral sites (0 0 0 and 0 0 $\frac{1}{2}$).

1. Introduction

Of the five known crystalline polymorphs of FeO(OH)‡, four are antiferromagnetic with well-established crystal and magnetic structures [1–6]. The fifth polymorph, δ-FeO(OH), is ferrimagnetic and is in many respects the most interesting of the five, being always poorly crystallized with a structure which has only been determined to a rough approximation [7–9]. The amorphous $FeO(OH)\cdot xH_2O$ can be either antiferromagnetic or ferrimagnetic depending on the method of preparation; this material is unstable and alters with ageing to α-Fe_2O_3 and α-FeO(OH) [10].

Our interest in δ-FeO(OH) derived from the fact that this phase is one of the few ferrimagnetic materials which can be prepared in bulk in a superparamagnetic state [11, 12]. Its magnetic properties can vary widely and are strongly dependent on the precise details of the preparation procedure. Room temperature magnetization values from below 10 to above 40 emu g^{-1} have been reported [11, 12]. δ-FeO(OH) can be prepared by several methods, including [13]:

(1) very rapid bubbling of oxygen through a suspension of $Fe(OH)_2$;

(2) rapid oxidation of $Fe(OH)_2$ with H_2O_2 or other peroxides or persulphates in an aqueous suspension;

(3) exposure of dried $Fe(OH)_2$ to oxygen.

The second of the above methods is by far the most commonly used, but the many published variants [7–9, 11–15] can still lead to a wide variety of different magnetic properties and degrees of crystallization.

Relatively little is known about δ-FeO(OH)-based solid solutions. Okamoto [16] reported the replacement of iron with various amounts of substituents: 50 at% Mn, 30 at% Ni, 15 at% Co, 30 at% Mg, 20 at% Zn and 15 at% Cd. Electrolytic oxidation of Fe–M alloys (M = Ni, Co, Mn) was used by Petit [17] to prepare the corresponding δ-FeO(OH)-based materials. Whereas the above solid solutions have been indexed on the basis of a δ-FeO(OH)-type unit cell (a CdI_2-type derivative), the $\frac{1}{3}$ Ni-substituted material has been indexed on the basis of the larger $CdCl_2$-type cell [18].

*Present address: Department of Chemical Engineering, Pennsylvania State University, University Park, Pennsylvania 16802, USA.

†Present address: IBM Corporation, Thomas J. Watson Research Center, P.O. Box 218, Yorktown Heights, New York 10598, USA.

‡These five include α-FeO(OH) or goethite [1, 2], β-FeO(OH) or akaganeite [3], γ-FeO(OH) or lepidocrocite [4], δ-FeO(OH) [7–9] and the high pressure form with the InO(OH) structure [5, 6].

0022–2461/79/122929–08$02.80/0

With only limited information available on the δ-FeO(OH) solid solutions, we felt that a more thorough study was in order. In the first of this series of papers, we describe the preparation and crystal chemistry of δ-FeO(OH)-type solid solutions of the type $Fe_{1-x}M_xO_{1-x}(OH)_{1+x}$ where M = Zn, Mg, Cd and Ca. In the second paper, a detailed transmission electron microscope (TEM) study of δ-FeO(OH) is presented. A third paper will deal with an X-ray and TEM study of the thermal decomposition of $Fe_{1-x}M_xO_{1-x}(OH)_{1+x}$, while a final paper will deal with the magnetic properties of these products.

An added incentive for a more thorough investigation is given by the fact that according to the latest structural study [7], the two antiferromagnetically coupled magnetic sublattices are almost equally populated with Fe^{3+} ions, giving rise to relatively low magnetization values. By substituting other ions for Fe^{3+} in the δ-FeO(OH) structure, a greater imbalance can be created between the sublattices with an accompanying increase in the magnetization values [16].

2. Methods of preparation and characterization

Our preliminary experiments in the preparation of δ-FeO(OH) and its solid solutions confirmed previous reports that the magnetic properties and crystallinity of δ-FeO(OH) are both very sensitive to small variations in the preparative method used. Therefore, we decided to follow a rigid procedure for making the bulk of our samples.

Reagent grade $FeSO_4 \cdot 7H_2O$ and the other hydrated matal sulphates* were weighed out in the appropriate ratio, dissolved in distilled water, after which the solution is flushed with nitrogen for at least 10 min to eliminate most of the residual oxygen. A 2N NaOH solution is similarly flushed with nitrogen.† Then, while being magnetically stirred, 80 ml 2N NaOH are added to 120 ml containing 0.04 mol of the mixed, dissolved sulphates. All this still takes place under a flow of nitrogen. This results initially in the formation of a precipitate of the type $Fe_{1-x}M_x(OH)_2$ which is initially nearly white but turns green, due to small amounts of Fe^{2+} being oxidized to Fe^{3+}. Such a small amount of oxidation is acceptable since the precipitate stays single phase up to 10% Fe^{3+} [19], or even 20% Fe^{3+} [9], and a continuous flow of nitrogen keeps the precipitate from oxidizing beyond the 10% Fe^{3+} stage.‡ The colloidal precipitate is now placed in a hot water bath and brought up to 60° C within about 5 min, after which it is oxidized with 30 ml 30% H_2O_2, added in 10 ml increments.§ This results in the rapid oxidation of Fe^{2+} to Fe^{3+}; i.e. paramagnetic $Fe_{1-x}M_x(OH)_2$ is converted to ferrimagnetic $Fe_{1-x}M_xO_{1-x}(OH)_{1+x}$. The M^{2+} ions remain in the divalent oxidation state. The resulting slurry is poured into cold tap water and stirred to help the coagulation process. The precipitate is then washed by decantation at least ten times with 2000 ml portions of deionized water. After filtering, the sample is air-dried for about 2 days, crushed to a fine powder using pestle and mortar, and dried in a vacuum desiccator over P_2O_5 for several hours. The samples were then kept in a drying cabinet until needed.

The X-ray diffraction patterns were taken with a Siemens Diffractometer using glass slide mounts and internal standards. A planimeter was used to obtain integrated intensities. The specimen preparation and instrumental techniques used for the TEM studies are described in the second paper of this series.

An elemental analysis was carried out on the $Fe_{1-x}M_xO_{1-x}(OH)_{1+x}$ samples. In addition to the metal ion analyses (Fe, Zn, Mg, Cd, Ca), thermogravimetric (TGA) traces were taken to determine the adsorbed water and structurally bound water. A few samples were analysed for Na and S in order to determine if traces of these elements had been introduced into the final products by the sulphate precursors and the NaOH. Elemental analyses were carried out by atomic absorption and X-ray fluorescence techniques.

In general, we found that the Fe/M ratio initially present in the precursor sulphate solution was retained in the final product. The compositions given

*For making Ca-substituted solid solutions, the hydrated chlorides were used since $CaSO_4$ is insoluble in water.

†For the Ca-substituted solid solutions, 11.3N NaOH solution was used.

‡According to Okamoto [7] small amounts of Fe^{3+} (~ 5%) in the $Fe(OH)_2$ precursor yield magnetic δ-FeO(OH) products which are more highly magnetic. In contrast, Powers [12] goes to great lengths to exclude any trace of Fe^{3+} in the $Fe(OH)_2$ precursor.

§This reaction is quite vigorous. To avoid spillages, a tall reaction vessel is recommended for the precipitation and oxidation reactions.

in this paper are those determined analytically. Here, the ideal formula $Fe_{1-x}M_xO_{1-x}(OH)_{1+x}$ will be used, although traces of sulphur (0.01 to 0.15 wt% S) and Na (0.02 to 0.10 wt% Na) were found in all samples analysed. From the TGA traces, 1 to 3 wt% adsorbed water was found in most samples. The relatively large quantities of adsorbed water in these phases is not unexpected due to the extremely finely divided state of these samples.

3. Results and discussion

The results of our experiments are summarized in Fig. 1, where the extent of the $Fe_{1-x}M_xO_{1-x}(OH)_{1+x}$ solid solution region is shown as a function of composition. It can be seen that the solid solubilities found in our study are larger than those observed by Okamoto for M = Zn, Mg, Cd [16]. This difference can be attributed to differences in the method of preparation, and the greater scarcity of data points of the Japanese study [16]. The solid solubility limits of the δ-FeO(OH) phases shown in Fig. 1 have been conservatively estimated and may extend toward still higher M-contents. However, we were unable to synthesize single phase solid solutions beyond $x = 0.35$.

Unit cell parameters are plotted in Fig. 2 for the $Fe_{1-x}Zn_xO_{1-x}(OH)_{1+x}$ solid solutions and a more detailed compilation is given in Table I for all $Fe_{1-x}M_xO_{1-x}(OH)_{1+x}$ phases. These phases can all be indexed on the basis of a δ-FeO(OH)-type unit cell. The hexagonal cell parameters increase with growing M^{2+} content since the divalent M^{2+} ions have larger ionic radii than Fe^{3+}. As expected, the largest increases in the cell parameters occur for $M = Cd^{2+}$, with its larger ionic radius than Mg^{2+} or Zn^{2+}. In general, the higher the M^{2+} content, the more poorly crystallized the $Fe_{1-x}M_xO_{1-x}(OH)_{1+x}$ solid solutions become as seen from the X-ray line broadening.* In most cases, the $h\,k\,0$ lines (1 0 0 and 1 1 0) are sharper than the other lines. Peaks having a high l index (such as the 0 1 2 reflection) are especially diffuse owing to the crystalline disorder and the thin nature of these hexagonal platelets in the c-direction.

The plate-like morphology of these materials can be seen from Fig. 3 and 4. δ-FeO(OH) occurs in hexagonal platelets 100 to 800 Å across (Fig. 3a) and 20 to 80 Å thick (Fig. 3b).† Similar crystal habits and even larger particle sizes are found for the Zn-substituted solid solutions illustrated in Fig. 4 for the $Fe_{0.67}Zn_{0.33}O_{0.67}(OH)_{1.33}$ composition. From Fig. 4b we can see that the platelets of $Fe_{0.67}Zn_{0.33}O_{0.67}(OH)_{1.33}$ are thicker than those of unmodified δ-FeO(OH). Both phases show sharp hexagonal outlines of the platelets with an apparent pitted surface structure. There is a tendency for the platelets to stick together along

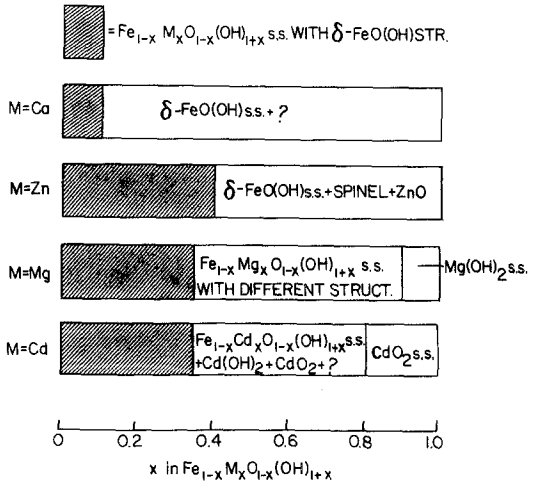

Figure 1 Extent of the solid solution range of δ-FeO(OH)-type phases of composition $Fe_{1-x}M_xO_{1-x}(OH)_{1+x}$.

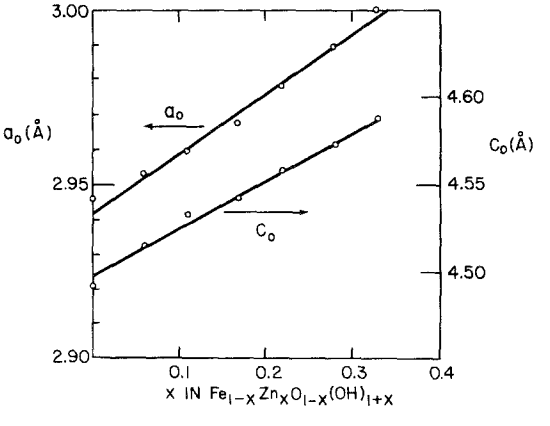

Figure 2 Hexagonal unit cell parameters for δ-FeO(OH)-type phases in the system $Fe_{1-x}Zn_xO_{1-x}(OH)_{1+x}$.

*The Zn-substituted solid solutions are an exception to this rule.

†A much more detailed TEM study is given in the second and third papers of this series for δ-FeO(OH) and substitutional decomposition products, respectively.

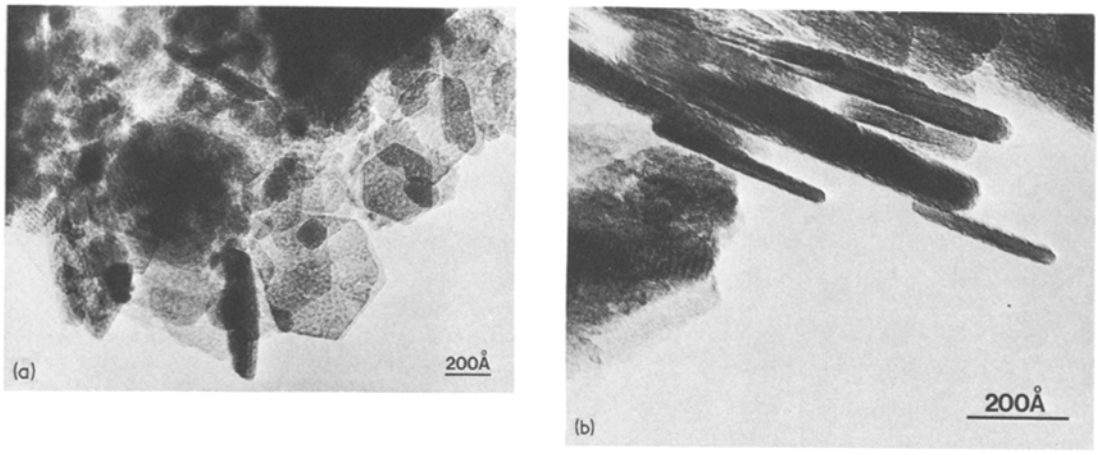

Figure 3 Transmission electron micrographs of δ-FeO(OH) showing shape and size distribution of crystalline plates. (a) Top view. (b) Edge-on view.

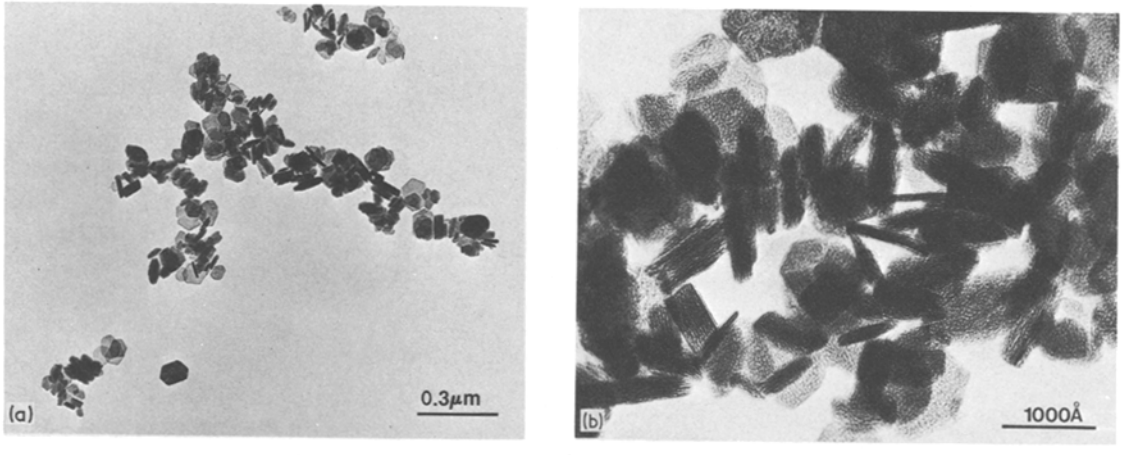

Figure 4 (a) Survey micrograph of $Fe_{0.67}Zn_{0.33}O_{0.67}(OH)_{1.33}$ showing shape and size distribution. (b) Higher magnification view.

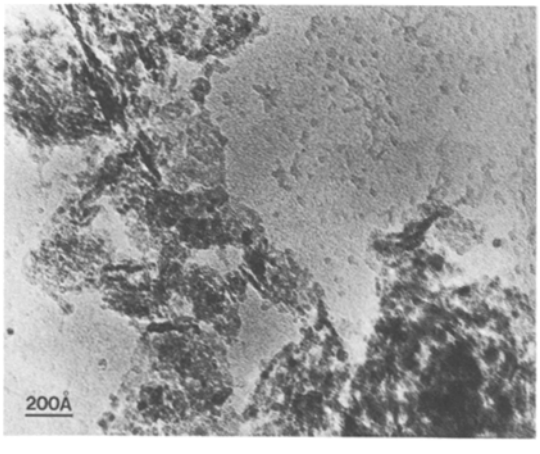

Figure 5 Electron micrograph of $Fe_{0.17}Mg_{0.83}O_{0.17}(OH)_{1.83}$.

their basal planes to form clusters. Such clusters are sometimes found stacked on edge as seen from Fig. 3b. Substantial substitution of Mg or Cd in $Fe_{1-x}M_xO_{1-x}(OH)_{1+x}$ gives rise to smaller and more irregularly shaped platelets, as illustrated in Fig. 5 for the $Fe_{0.17}Mg_{0.83}O_{0.17}(OH)_{1.83}$ composition. Here we have particles which may be only 20 to 40 Å diameter and it is, therefore, not surprising that such phases give rise to extremely broad X-ray peaks.

As indicated in Fig. 1, the $Fe_{0.17}Mg_{0.83}O_{0.17}(OH)_{1.83}$ composition corresponds to a phase (or phases) with a structure different from (but related to) $Mg(OH)_2$ and δ-FeO(OH). A tentative interpretation of the X-ray data in the intermediate region of $Fe_{1-x}Mg_xO_{1-x}(OH)_{1+x}$ (with $0.35 \leqslant x \leqslant 0.90$) can be made in terms of a

mixture of two phases of variable composition, one corresponding to a phase isotypic with green rust I [9] with Mg^{2+} replacing Fe^{2+} in green rust I. The other phase in the mixture corresponds to either a $Mg(OH)_2$ or δ-FeO(OH) solid solution, depending on the composition. The green rust I phase could not be obtained in a pure state. From Fig. 5 it would appear that both phases are very finely divided and cannot be distinguished in the electron micrograph.

In the $Fe_{1-x}Cd_xO_{1-x}(OH)_{1+x}$ system, an interesting observation has been made for a phase near $x = 0.8$. The X-ray pattern for this phase corresponds to a pyrite-type CdO_2 pattern [20] with cell parameters which are comparable to those of CdO_2.* Since no other X-ray peaks were found, we assume that the Fe^{3+} has entered the pyrite structure of CdO_2. This would be unusual, since transition metal ions rarely form peroxides and to our knowledge Fe^{3+} has not been reported in any inorganic peroxide structure.

4. Structural considerations

The structure of δ-FeO(OH) has been explored by Francombe and Rooksby [8] who favoured a disordered CdI_2-related structure with 20% of the Fe^{3+} ions occupying randomly the tetrahedral sites and the remaining 80% distributed among both octahedral sites. While a Mössbauer study [21] is not inconsistent with a partial tetrahedral occupancy, a more recent structure proposal by Okamoto [7] suggests that the X-ray peak intensities and magnetic data can best be accounted for by assuming a partial and nearly equal Fe^{3+} occupancy of two octahedral sublattices. This structure model is in good agreement with the extremely weak (or absent) 0 0 1 peak in the δ-FeO(OH) patterns and with an assumption of antiferromagnetic coupling between the two octahedral sublattices. Okamoto's model [7] postulates no significant tetrahedral occupancy of Fe^{3+} in the δ-FeO(OH) structure.

To check the validity of these structural models, we have carried out some trial intensity calculations using a programme designed for powder patterns [22]. In comparing X-ray powder data for the $Fe_{1-x}M_xO_{1-x}(OH)_{1+x}$ phases (M = Cd, Mg, Zn) we observe no detectable 0 0 1 peak for $0 \leqslant x \leqslant 0.12$ and for all values of x where M = Cd. Trial X-ray intensity calculations for such phases are in reasonable agreement with the Okamoto model [7] suggesting that there is only a small imbalance in the cation occupation of the two octahedral sublattices, e.g. 55% occupancy of the 0 0 0 site and 45% occupancy of the $0\,0\,\frac{1}{2}$ site. Such a small imbalance would yield 0 0 1 peak intensities of the order of 2% which would be unobservable in these weak and diffuse X-ray scans.

In the systems $Fe_{1-x}M_xO_{1-x}(OH)_{1+x}$ with M = Mg and Zn, the 0 0 1 peak becomes barely observable for $x = 0.17$ and increases in intensity with increasing x. While the 0 0 1 peak is very diffuse for the Mg-substituted phases, this peak is sharper for $Fe_{1-x}Zn_xO_{1-x}(OH)_{1+x}$ due to the greater thickness of the hexagonal platelets. In Fig. 6 we compare portions of the X-ray

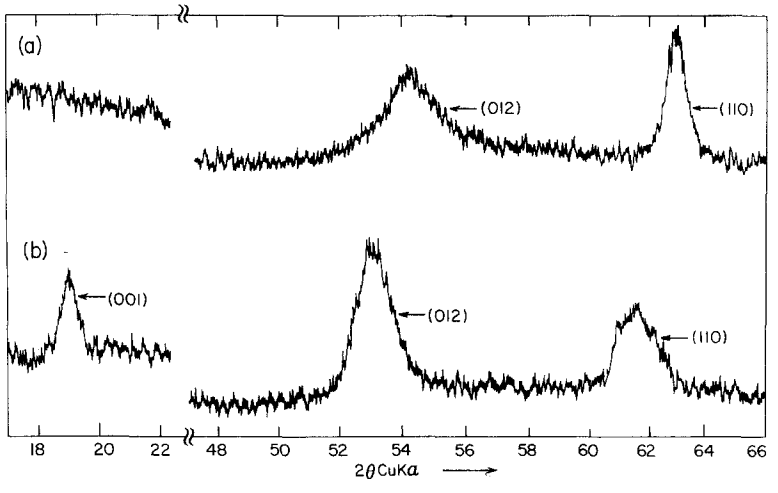

Figure 6 Partial X-ray diffraction trace of (a) δ-FeO(OH) and (b) $Fe_{0.67}Zn_{0.33}O_{0.67}(OH)_{1.33}$.

* Pure CdO_2 has never been made. The actual composition is near $Cd(O_2)_{0.88}(OH)_{0.24}$ [20].

traces for unsubstituted δ-FeO(OH) and $Fe_{0.67}Zn_{0.33}O_{0.67}(OH)_{1.33}$. A number of differences between the two patterns are observed. The absence of the 0 0 1 in the δ-FeO(OH) and the clear presence of this peak in $Fe_{0.67}Zn_{0.33}O_{0.67}(OH)_{1.33}$ are attributable to structural and compositional differences, as will be discussed below. There is a shift to the left in the 0 1 2 and 1 1 0 peaks with increasing Zn-substitution, which is a consequence of the larger cell parameters (see Table I and Fig. 2). Finally, it is instructive to compare the 0 1 2 peaks. This peak is very broad in δ-FeO(OH) due to the extremely thin nature of the hexagonal platelets (20 to 50 Å thick) as seen from Fig. 3. In contrast, these platelets are thicker for the Zn substituted material (Fig. 4), giving rise to a sharper 0 1 2 peak. As seen from Fig. 6, there are significant changes in the background intensity especially around the 0 1 2 peak. This makes it difficult to measure accurately the true peak intensities.

Owing to their better crystallinity, the $Fe_{1-x}Zn_xO_{1-x}(OH)_{1+x}$ phases (with $0 \leqslant x \leqslant 0.33$) were used for trial X-ray intensity calculations. A variety of models were used, including variations based on the Okamoto [7] and Francombe–Rooksby [8] models. As in the previous models, good intensity agreement could not be attained since the observed $h\,k\,0$ reflections were anomalously strong when compared to the observed $h\,k\,l$ reflections.* A similar trend has been found by Okamoto for δ-FeO(OH) [7] and by Hoekstra *et al.* for α-PtO_2 [23], which also has a disordered CdI_2-type structure. We attribute this trend to the presence of lattice defects along the hexagonal c-direction, which disrupt the crystalline periodicity and cause a weakening in the $h\,k\,l$ lines and most of all in the 0 0 1 lines.† If this tendency is taken into consideration, a satisfactory model emerges if we place the atoms as follows in space group D_{3d}^3-$P\bar{3}m1$, as given in the "International Tables for X-ray Crystallography":

x Zn in (a) 0 0 0

$\frac{1}{2}(1-x)$ Fe in (a) 0 0 0

$\frac{1}{2}(1-x)$ Fe in (b) 0 0 $\frac{1}{2}$

$\left.\begin{matrix}(1-x)\ \mathrm{O} \\ (1+x)\ \mathrm{OH}\end{matrix}\right\}$ in (d) $\frac{1}{3}\,\frac{2}{3}\,\frac{1}{4}, \frac{2}{3}\,\frac{1}{3}\,\frac{3}{4}$.

Since the 0 0 1 reflection is the most sensitive with respect to the cation distribution among the two octahedral sublattices, we compare in Fig. 7 the calculated with the observed integrated 0 0 1 intensities based on this model. We see that with increasing Zn-content there is an increase in the 0 0 1 intensity and hence a growing imbalance between the occupancies of the two octahedral sites. As can be seen, the curves are roughly parallel with the observed intensities weaker than expected for reasons cited above.

The following picture emerges from this model. As the $Fe_{1-x}Zn_x(OH)_2$ solid solutions are first precipitated, the Fe^{2+} and Zn^{2+} ions occupy randomly (but fully) the 0 0 0 octahedral site of the CdI_2 structure, leaving the 0 0 $\frac{1}{2}$ site empty. This is illustrated in Fig. 8 for δ-FeO(OH). As the precipitates are oxidized with H_2O_2, the Zn^{2+} ions stay behind in the 0 0 0 site, but about half‡ of the newly oxidized Fe^{3+} ions move to the other octahedral site at 0 0 $\frac{1}{2}$, as shown in Fig. 8b. This is a very rapid and almost violent reaction which involves the effective loss of a proton in the replacement of O^{2-} ions for some OH^- ions. This sudden structural and compositional change apparently causes severe structural disturbances and a reduction of the atomic order especially along the c-axis, as many ions are displaced from their ideal positions. Such a partial disorder would

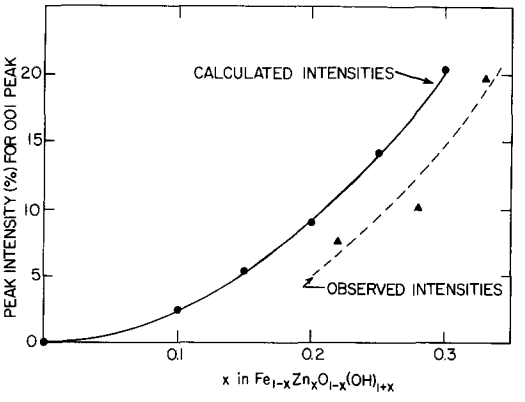

Figure 7 Comparison of calculated and observed 0 0 1 peak intensities for $Fe_{1-x}Zn_xO_{1-x}(OH)_{1+x}$.

*Observed $h\,k\,0$ peaks are typically 30% to 50% more intense than calculated $h\,k\,0$ lines. All peak intensities are relative to the 0 1 2 line ($I = 100\%$) which is the most intense reflection.

†The very thin nature of the hexagonal platelets should give rise to broader (but not weaker) X-ray peaks, if a high degree of crystalline order is assumed.

‡ The exact fraction is probably variable and depends on the method of preparation.

TABLE I Unit cell parameters for the hexagonal $Fe_{1-x}M_xO_{1-x}(OH)_{1+x}$ phases with the δ-FeO(OH) structure

M	x	a_0(Å)	c_0(Å)
–	0	2.946	4.492
Ca	0.05	2.966	4.581
Ca	0.10	2.979	4.651
Cd	0.05	2.969	4.542
Cd	0.12	2.987	4.592
Cd	0.18	3.008	4.629
Cd	0.24	3.028	4.678
Cd	0.34	3.072	4.775
Zn	0.06	2.953	4.515
Zn	0.11	2.960	4.534
Zn	0.17	2.968	4.542
Zn	0.22	2.978	4.558
Zn	0.28	2.990	4.573
Zn	0.33	3.000	4.588
Mg	0.06	2.952	4.514
Mg	0.11	2.959	4.532
Mg	0.17	2.969	4.538
Mg	0.23	2.977	4.543
Mg	0.27	2.985	4.559
Mg	0.32	2.992	4.579

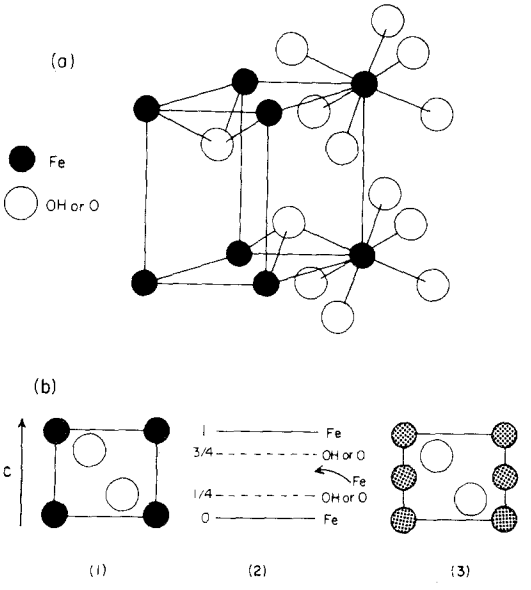

Figure 8 (a) The structure of $Fe(OH)_2$ (CdI_2-type). (b) Schematic diagram of the conversion of $Fe(OH)_2$ shown in (1) by moving of some Fe atoms into empty octahedral sites (2) and final δ-FeO(OH) structure (3) with all octahedral sites only partially occupied as shown by the lighter shading.

be difficult to model on an atomic basis since it is possible that larger subunits than atoms are involved.

In evaluating the structural model discussed above, one must recognize that the X-ray scattering powers for Zn and Fe are nearly the same. Therefore, this model cannot be easily distinguished from a more random one postulating a larger imbalance between Fe^{3+} ions between the two octahedral sublattices and with some Zn^{2+} ions in the $00\frac{1}{2}$ sites. However, the model postulated above is intuitively more satisfying in view of the near parallel trend of the two curves in Fig. 7.

Numerous intensity calculations were carried out assuming partial tetrahedral cation occupancy. In all cases a poorer intensity agreement was obtained. We must conclude, in accord with Okamoto [7], that any tetrahedral occupancy (if it exists at all) is very small and below the 20% level suggested by Francombe and Rooksby [8]. We must point out, however, that structural details for the δ-FeO(OH) phases may vary from sample to sample depending on the method of preparation. Hence the above discussion of the structural model is valid only for samples prepared in this study.

In the structural calculations we have assumed the anions to be located at $\frac{1}{3}\frac{2}{3}\frac{1}{4}$, $\frac{2}{3}\frac{1}{3}\frac{3}{4}$. However, the positional z-parameter is not fixed and normally varies between 0.22 and 0.24 for CdI_2-type $M(OH)_2$ with M = Cd, Mg, Ca [24]. We believe that in the δ FeO(OH) structure, z is very close to 0.25 since both octahedral sublattices are occupied in contrast to the hydroxides. In any case, small deviations from $z = 0.25$ will not significantly alter the X-ray intensities, as shown by trial calculations.

References

1. A. SZYTULA, A. BUREWICZ, Z. DIMITRIJEVIC, S. KRASNICKI, H. RZANY, J. TODOROVIC, A. WANIC and W. WOLSKI, *Phys. Stat. Sol.* **26** (1968) 429.
2. J. B. FORSYTH, I. G. HEDLEY and C. E. JOHNSON, *J. Phys. C* **1** (1968) 179.
3. A. SZYTULA, M. BALANDA and Z. DIMITRIJEVIC, *Phys. Stat. Sol. (a)* **3** (1970) 1033.
4. A. OLES, A. SZYTULA and A. WANIC, *ibid* **41** (1970) 173.
5. M. PERNET, J. CHENAVAS, J. C. JOUBERT, C. MEYER and Y. GROS, *Solid State Commun.* **13** (1973) 1147.
6. M. PERNET, J. C. JOUBERT and C. BERTHET-COLOMINAS, *ibid* **17** (1975) 1505.
7. S. OKAMOTO, *J. Amer. Ceram. Soc.* **51** (1968) 594.
8. M. H. FRANCOMBE and H. P. ROOKSBY, *Clay Minerals Bull.* **4** (1959) 1.
9. J. D. BERNAL, D. R. DASGUPTA and A. L. MACKAY, *ibid* **4** (1959) 15.

10. S. OKAMOTO, H. SEKIZAWA and S. I. OKAMOTO, "Reactivity of Solids", Proceedings of the 7th International Symposium on the Reactivity of Solids, Bristol (Chapman and Hall, London, 1972) p. 341.
11. A. W. SIMPSON, *J. Appl. Phys.* **33** Suppl. (1962) 1203.
12. D. A. POWERS, PhD Thesis, California Institute of Technology (1975).
13. W. FEITKNECHT, *Z. Electrochem.* **63** (1959) 34.
14. S. OKAMOTO, *Kogyo Kagaku Zasshi* **67** (1964) 1845.
15. *Idem, ibid* **67** (1964) 1850.
16. *Idem, ibid* **67** (1964) 1855.
17. J.-C. PETIT, *Compt. Rend.* **252** (1961) 3255.
18. S. OKAMOTO, *J. Amer. Ceram. Soc.* **51** (1968) 113.
19. W. FEITKNECHT and G. KELLER, *Z. Inorg. Chem.* **262** (1950) 61.
20. N. G. VANNERBERG, *Ark. Kemi* **10** (1956) 455.
21. I. DÉZSI, L. KESZTHELYI, D. KULGAWCZUK, B. MCINAR and N. A. EISSA, *Phys. Stat. Sol.* **22** (1967) 617.
22. C. M. CLARK, D. K. SMITH and G. G. JOHNSON, "A Fortran IV Program For Calculating X-Ray Powder Diffraction Patterns – Version 5, Pennsylvania state, University (1973).
23. H. R. HOEKSTRA, S. SIEGEL and F. X. GALLAGHER, *Adv. Chem. Series* **98** (1971) 39.
24. G. BERTRAND and Y. DUSAUSOY, *Compt. Rend.* **270C** (1970) 612.

Received 26 April and accepted 17 May 1979.